Finite Elements in Analysis and Design 227 (2023) 104023

Contents lists available at ScienceDirect

Finite Elements in Analysis & Design

journal homepage: www.elsevier.com/locate/finel

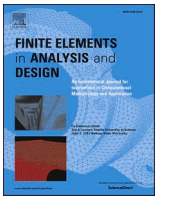

Ritz vector-based substructuring method using interface eigenmode-shape pseudo-forces

Hyeong Seok Koh, Gil Ho Yoon *

Mechanical Engineering, Hanyang University, Republic of Korea

ARTICLE INFO

Keywords:
Interfacial pseudo-force
Substructuring method
Krylov subspace
Ritz vector method
Quasi-static ritz vector method

ABSTRACT

We propose a new Ritz vector-based dynamic substructuring method which substitutes the unit pseudo-forces applied at the adjacent degrees of freedom (DOFs) using distributed forces. One of the main problems of the Ritz vector and unit pseudo-force-based dynamic substructuring method is the strong dependence of the number of reduction bases on the interface DOF, which is not reduced by substructuring. This type of dependency causes the number of reduction bases obtained by the unit pseudo-forces to be always exceed or at least equal to the number of interface DOFs. The number of Ritz vector bases required at adjacent interface DOFs is efficiently reduced by approximating the unit pseudo-force as a type of distributed force using an energy transfer approach. The distributed forces, called *eigenmode-shape pseudo-forces,* comprise low modes computed through the eigenvalue problem of substructures corresponding to adjacent DOFs, and a set of distributed forces is a subspace of the vector space spanned by the unit force vectors. The efficiency of the substructuring method may be increased by reducing the number of reduction bases. This approach was demonstrated through several numerical examples.

1. Introduction

This study presents a new dynamic substructuring method which introduces the idea of *eigenmode-shape pseudo-forces* for an efficient substructuring method based on quasi-static Ritz vectors. The model order reduction (MOR) method is essential for analyzing large-scale finite element (FE) models in various engineering fields. Despite developments in computer hardware and FE theory, the ever-increasing complexity of FE models hinders the calculation of FE responses in the time or frequency domains. Thus, the substructuring method, which is the MOR method for multiple components, is an important technique for resolving the issue of computational resources decomposing a complex system into subsystems, analyzing their responses independently, and integrating the responses. It is noteworthy that the substructuring method can significantly reduce the computational cost, especially for dynamic analyses using reduced substructural FE models instead of a large-scale original FE model (or full order model, FOM). Moreover, it plays a crucial role in various engineering design fields where full models comprise multiple components, and each component is independently analyzed and designed. Comprehensive reviews of substructuring methods have been studied for their efficiency and accuracy [1–6].

Various substructuring techniques have been developed for calculating mechanical responses. In the early 1960s, Hurty presented a method for analyzing structural systems, in which the displacement of each substructure was described by three types of generalized

* Corresponding author. School of Mechanical Engineering, Hanyang University, Seoul, Republic of Korea.
E-mail address: ghy@hanyang.ac.kr (G.H. Yoon).

https://doi.org/10.1016/j.finel.2023.104023
Received 3 April 2023; Received in revised form 6 August 2023; Accepted 23 August 2023
Available online 6 September 2023

coordinates (i.e., modes): rigid body coordinate, constraint coordinate, and normal mode coordinate [7,8]. Guyan developed a mode condensation method by splitting the total degree of freedom (DOF) of an original system into primary (master) and secondary (slave) DOF [9]. Based on Hurty and Guyan's suggestion, Craig and Bampton developed a new substructuring method, known as the Craig–Bampton (CB) method, which excluded rigid body motions if all the interface degrees of freedom were included in the component modes [10]. Various studies derived from the CB method have been conducted to improve the accuracy performance [1,3,6,11–22]. These methods are known as *component mode synthesis* (CMS), where the term *modes* includes all kinds of structural modes, such as exact eigenmodes, static modes, interface modes, and approximated (or assumed) modes. However, the performance of exact eigenmodes-based CMS methods deteriorated in the high- or mid-frequency ranges, because they are based on the mode superposition (MS) theory, which truncates low- or high-frequency modes. This can be disadvantageous, especially for frequency response analysis (FRA), which requires high accuracy over a wide frequency range. Various studies have been conducted to select the appropriate eigenmodes and truncate useless eigenmodes, such as the frequency cutoff technique [8,23,24]. Meanwhile, assumed modes (in fact, Ritz vectors)-based methods that substitute the eigenmodes of the MS theory with (quasi-) static displacement around a frequency of interest have been developed as an alternative to the MS method [25–30]. A few substructuring methods derived from the RV method have been developed. Ma and Hulbert presented the quasi-static Ritz vector and quasi-static mode compensation methods [19,31]. Craig and Hale tried to adopt a Ritz vector for computational efficiency [12]; however, static displacement or eigenmodes were still inevitably used as inertia force terms for generating Ritz vectors without external loads.

One of the main problems in replacing exact eigenmodes with Ritz vectors is the lack of proper boundary conditions and external

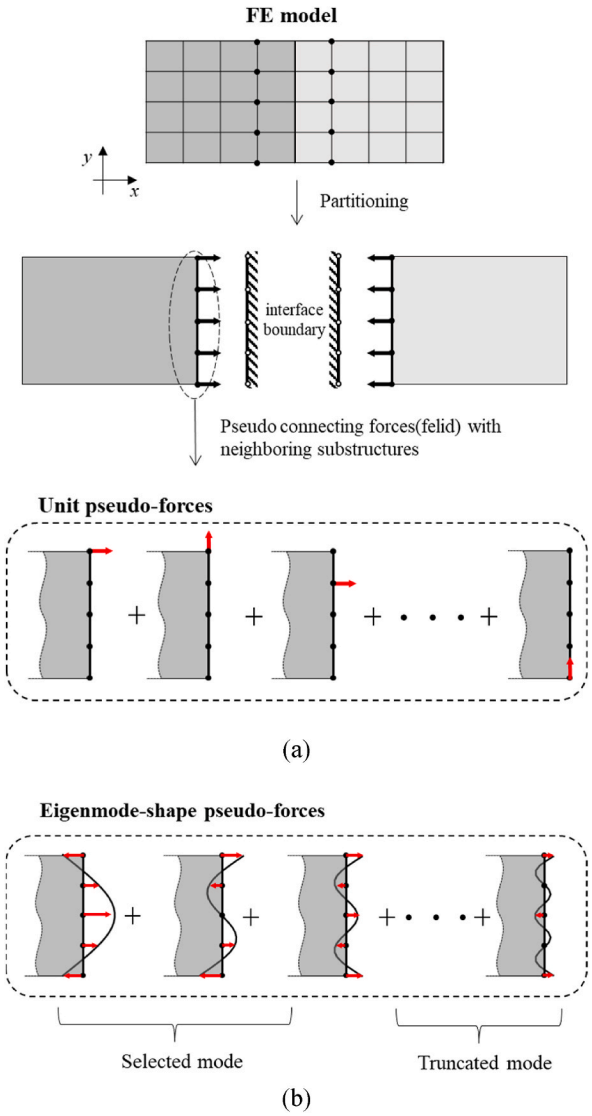

Fig. 1. Schematic of the pseudo-force based-substructuring method. (a) Substructuring approach and the concept of unit pseudo-forces and (b) proposed *eigenmode-shape pseudo-forces*.

load terms to obtain the Ritz vectors. A pseudo-force concept, defined by specifying a unit force (load) at one adjacent boundary degree of freedom (DOF) while fixing the actual boundary DOFs, was proposed in our previous work to resolve this problem (as shown in Fig. 1 (a)). These types of forces (loads) and corresponding displacement shapes are called the unit pseudo-forces and pseudo-attachment modes, respectively [32]. However, with FE model complex interfaces, the number of bases accounting for the unit pseudo-forces is significantly increased, which deteriorates the associated computational efficiency. Therefore, this study aims at approximating the unit pseudo-force as a specific distributed force by considering the interaction energy transferred between the substructures for an efficient Ritz vector-based substructuring method. As shown in Fig. 1 (b), the distributed force, called the *eigenmode-shape pseudo-force*, consists of truncated eigenmodes computed through the eigenvalue problem of substructures corresponding to adjacent DOFs, and a set of distributed force vectors is a subspace of the vector space spanned by the unit force vectors.

The remainder of this study is organized as follows: First, the basic concepts of the substructuring techniques are reviewed. Then, we present a new substructuring method based on the concept of *eigenmode-shape pseudo-forces*. The performance and characteristics of the present method are numerically studied using two-dimensional (2D) and three-dimensional (3D) structures. The concluding section summarizes the findings and future research topics.

2. Overview of the conventional dynamic substructuring method

2.1. Equilibrium equations of a dynamic system

Newton's second equation is solved for the time-varying response of a linear solid structure with a time-varying force, .

$$\mathbf{M}\ddot{\mathbf{u}}(t) + \mathbf{C}\dot{\mathbf{u}}(t) + \mathbf{K}\mathbf{u}(t) = \mathbf{f}(t) \tag{1}$$

where, $\mathbf{C}$, and $\mathbf{K}$ are the mass, damping, and stiffness matrices with appropriate boundary conditions [33], respectively. The time-varying displacement, velocity, and acceleration vectors are represented by $\mathbf{u}(t)$, $\dot{\mathbf{u}}(t)$, and. $\ddot{\mathbf{u}}(t)$., respectively. For simplicity, the following Rayleigh damping with damping coefficients α_r and β_r is assumed.

$$\mathbf{C} = \alpha_r\mathbf{M} + \beta_r\mathbf{K} \tag{2}$$

The following harmonic response and excitation were assumed to compute the frequency response of the system.

$$\mathbf{u}(t) = \mathbf{u}e^{j\omega t}, \mathbf{f}(t) = \mathbf{f}e^{j\omega t} \tag{3}$$

The dynamic stiffness matrix $\mathbf{D}$ is defined for the solution.

$$\mathbf{D} = \mathbf{K} + j\omega\mathbf{C} - \omega^2\mathbf{M} \text{ and} \tag{4}$$

2.2. General framework of the substructuring approach

The analysis of large-scale models comprising a significant number of subcomponents is difficult at a moderate computational cost, even by the most advanced and state-of-the-art computational systems. These difficulties can be overcome by a method that reduces the dynamic problem without modifying the mesh. Such methods are called reduction methods (or Model Order Reduction) and similar to modal superposition, the full set of DOFs (physical domain) is approximated by a set of possible displacement shapes and corresponding amplitudes called the generalized DOFs (generalized domain).

The approximated displacement vector $\tilde{\mathbf{u}}$ of the original displacement vector $\mathbf{u}$ and its generalized coordinate can be defined as:

$$\mathbf{u} \approx \tilde{\mathbf{u}} = \mathbf{R}\mathbf{q} \tag{5}$$

For a system with n degrees of freedom, $\mathbf{R} \in \mathbb{R}^{n\times m}(m < n)$ where m is dimension of approximated model. In addition to exact eigenmodes, all kinds of structural modes (i.e., eigenmodes, static modes, interface modes, approximated modes, etc.) can be used to generate the reduction basis $\mathbf{R}$.

The substructuring approach extends this reduction scheme to a system comprising multiple substructures. To explain the principles of the substructuring scheme, we consider a finite element model defined on a global domain Ω, which is divided into N_s , each spanning a subdomain $\Omega^{(s)}$ and interface boundary Γ. The undamped equations of motion in subdomain $\Omega^{(s)}$ can be written as:

$$\mathbf{M}^{(s)}\ddot{\mathbf{u}}^{(s)}(t) + \mathbf{K}^{(s)}\mathbf{u}^{(s)}(t) = \mathbf{f}^{(s)}(t) + \mathbf{g}^{(s)}(t) \tag{6}$$

where the superscript (s) denotes the particular substructure s, and $\mathbf{g}^{(s)}$ is the vector of connecting (or interactional) forces with the neighboring substructures.

Using the generalized set of DOFs in Eq. (5), a system possessing n degrees of freedom (6) can be reduced.

$$\mathbf{M}^{(s)}\mathbf{R}^{(s)}\ddot{\mathbf{q}}^{(s)} + \mathbf{K}^{(s)}\mathbf{R}^{(s)}\mathbf{q}^{(s)} = \mathbf{f}^{(s)} + \mathbf{g}^{(s)} + \mathbf{r}^{(s)} \tag{7}$$

where $\mathbf{r}^{(s)}$ is the error or residual load because the generalized DOFs do not span the entire solution space; it represents the approximation error in Eq. (5). The inner product of $\mathbf{r}^{(s)}$ with any subspace spanned by the reduction basis $\mathbf{R}^{(s)}$ is zero because the error represents the part of the equation that lies outside the subspace of the reduction basis (i.e., ${\mathbf{R}^{(s)}}^{\mathrm{T}}\mathbf{r}^{(s)} = \mathbf{0}$). To simplify the notation, the

time notation (t) will be omitted hereafter. Using this property, the reduced equations of motion can be expressed as follows:

$$\widetilde{\mathbf{M}}^{(s)}\ddot{\mathbf{q}}^{(s)} + \widetilde{\mathbf{K}}^{(s)}\mathbf{q}^{(s)} = \widetilde{\mathbf{f}}^{(s)} + \widetilde{\mathbf{g}}^{(s)} \tag{8}$$

where,

$$\begin{cases} \widetilde{\mathbf{M}}^{(s)} = \mathbf{R}^{(s)^{\mathrm{T}}}\mathbf{M}^{(s)}\mathbf{R}^{(s)} \\ \widetilde{\mathbf{K}}^{(s)} = \mathbf{R}^{(s)^{\mathrm{T}}}\mathbf{K}^{(s)}\mathbf{R}^{(s)} \\ \widetilde{\mathbf{f}}^{(s)} = \mathbf{R}^{(s)^{\mathrm{T}}}\mathbf{f}^{(s)} \\ \widetilde{\mathbf{g}}^{(s)} = \mathbf{R}^{(s)^{\mathrm{T}}}\mathbf{g}^{(s)} \end{cases} \tag{9}$$

The above procedures project the equations of motion in physical coordinates onto the reduction basis $\mathbf{R}^{(s)}$. Thus, the reduction basis $\mathbf{R}^{(s)}$ acts as a transformation matrix that transforms a set of physical DOFs into a set of generalized DOFs. However, coupling the approximated substructures using generalized DOFs is quite difficult and rarely performed in substructuring procedures. Instead, the interface boundary DOFs are preserved rather than reduced. Distinguishing the internal and (interface) boundary DOFs leads to the following form of the equations of motion in physical coordinate (Eq. (6)):

$$\mathbf{M}^{(s)} = \begin{bmatrix} \mathbf{M}_{ii} & \mathbf{M}_{ib} \\ \mathbf{M}_{bi} & \mathbf{M}_{bb} \end{bmatrix}^{(s)} \mathbf{K}^{(s)} = \begin{bmatrix} \mathbf{K}_{ii} & \mathbf{K}_{ib} \\ \mathbf{K}_{bi} & \mathbf{K}_{bb} \end{bmatrix}^{(s)} \mathbf{u}^{(s)} = \begin{bmatrix} \mathbf{u}_i \\ \mathbf{u}_b \end{bmatrix}^{(s)} \mathbf{f}^{(s)} = \begin{bmatrix} \mathbf{f}_i \\ \mathbf{f}_b \end{bmatrix}^{(s)} \mathbf{g}^{(s)} = \begin{bmatrix} \mathbf{0} \\ \mathbf{g}_b \end{bmatrix}^{(s)} \tag{10}$$

For a common denominator for the coupling substructures, the DOFs on the interface boundaries of the substructures are preserved, and only the DOFs on the internal substructures $\mathbf{u}_i^{(s)}$ are reduced to a generalized coordinate $\mathbf{q}^{(s)}$ Therefore, the approximated equations of motion in Eq. (5) are:

$$\begin{bmatrix} \mathbf{u}_i \\ \mathbf{u}_b \end{bmatrix}^{(s)} \approx \begin{bmatrix} \mathbf{R}_i \\ \mathbf{R}_b \end{bmatrix}^{(s)} \mathbf{q}^{(s)} \text{ where, } \mathbf{q}^{(s)} = \begin{bmatrix} \mathbf{q}_i \\ \mathbf{q}_b = \mathbf{u}_b \end{bmatrix}^{(s)} \tag{11}$$

The detailed method for obtaining the reduction basis is described in Section 2.3.

After reducing the equations of motion, each substructure was assembled under the following two conditions.

1) Compatibility: the displacements of the substructures at the interface boundary DOFs ($\mathbf{q}_b$) must be identical.
2) Equilibrium: the sum of the interactional forces between neighboring substructures ($\mathbf{g}_b$) must be equal to zero.

A primal or dual-assembled system is obtained depending on whether a compatibility or equilibrium condition is chosen. However, only the primal-assembled system is described in this work.

Following the equations of motion at the substructure level, the global equations of motion that have not yet been assembled can be expressed in the form of a block-diagonal matrix:

$$\widetilde{\mathbf{M}}\ddot{\mathbf{q}} + \widetilde{\mathbf{K}}\mathbf{q} = \widetilde{\mathbf{f}} + \widetilde{\mathbf{g}} \tag{12}$$

where,

$$\begin{aligned} &\widetilde{\mathbf{M}} = \mathrm{diag}\left(\widetilde{\mathbf{M}}^{(1)}, \ldots, \widetilde{\mathbf{M}}^{(N_s)}\right) = \begin{bmatrix} \widetilde{\mathbf{M}}^{(1)} & \cdots & \mathbf{0} \\ \vdots & \ddots & \vdots \\ \mathbf{0} & \cdots & \widetilde{\mathbf{M}}^{(N_s)} \end{bmatrix}, \\ &\widetilde{\mathbf{K}} = \mathrm{diag}\left(\widetilde{\mathbf{K}}^{(1)}, \ldots, \widetilde{\mathbf{K}}^{(N_s)}\right), \\ &\mathbf{q} = \begin{bmatrix} \mathbf{q}^{(1)} \\ \vdots \\ \mathbf{q}^{(N_s)} \end{bmatrix}, \widetilde{\mathbf{f}} = \begin{bmatrix} \widetilde{\mathbf{f}}^{(1)} \\ \vdots \\ \widetilde{\mathbf{f}}^{(N_s)} \end{bmatrix}, \widetilde{\mathbf{g}} = \begin{bmatrix} \widetilde{\mathbf{g}}^{(1)} \\ \vdots \\ \widetilde{\mathbf{g}}^{(N_s)} \end{bmatrix} \end{aligned} \tag{13}$$

Next, the compatibility condition can be written in matrix form as:

$$\mathbf{B}\mathbf{q} = \mathbf{0} \tag{14}$$

where $\mathbf{B}$ is a signed Boolean matrix (if the interface DOFs match with each other) operating on the interface DOFs of the substructures. The rows of $\mathbf{B}$ state that any pair of matching interface DOFs $q^{(k)}$ and $q^{(l)}$ must have the same displacement, that is, $q^{(k)} - q^{(l)} = 0$.

Similar to the compatibility condition, the equilibrium condition can be written as:

$$\mathbf{L}^{\mathrm{T}}\widetilde{\mathbf{g}} = \mathbf{0} \tag{15}$$

where $\mathbf{L}$ is a Boolean matrix localizing the interface DOF of the substructures in the dual set of DOFs. The columns of $\mathbf{L}$ state that the sum of any pair of interface connecting forces $\widetilde{g}^{(k)}$ and $\widetilde{g}^{(l)}$ is equal to zero, that is, $\widetilde{g}^{(k)} + \widetilde{g}^{(l)} = 0$.

Hence, the total system is described by Eqs. 12–15:

$$\begin{cases} \widetilde{\mathbf{M}}\ddot{\mathbf{q}} + \widetilde{\mathbf{K}}\mathbf{q} = \widetilde{\mathbf{f}} + \widetilde{\mathbf{g}} \\ \mathbf{B}\mathbf{q} = \mathbf{0} \\ \mathbf{L}^{\mathrm{T}}\widetilde{\mathbf{g}} = \mathbf{0} \end{cases} \tag{16}$$

Mathematically, a set of unique interface DOFs is obtained by following statements:

$$\mathbf{q} = \mathbf{L}\overline{\mathbf{q}} \tag{17}$$

$$\widetilde{\mathbf{g}} = -\mathbf{B}^{\mathrm{T}}\boldsymbol{\lambda} \tag{18}$$

where $\overline{\mathbf{q}}$ represents the unique set of interface DOFs for the assembled system and $\boldsymbol{\lambda}$ are the Lagrange multipliers of d'Alembert's principle of virtual work, corresponding physically to the connecting (constraining) force intensity (as shown in Fig. 2). Using this statement in Eq. (17), the compatibility condition of Eq. (14) is satisfied for any set of $\overline{\mathbf{q}}$ (i.e., $\mathbf{B}\mathbf{L}\overline{\mathbf{q}} = \mathbf{0}\forall\overline{\mathbf{q}}$). Hence, the two Boolean matrices represent each other's null space, namely, $\mathbf{L} = \mathrm{null}(\mathbf{B}), \mathbf{B}^{\mathrm{T}} = \mathrm{null}(\mathbf{L}^{\mathrm{T}})$. Because the compatibility condition is satisfied by the choice of DOFs in the unique set $\overline{\mathbf{q}}$, the system is described by

$$\begin{cases} \widetilde{\mathbf{M}}\mathbf{L}\ddot{\overline{\mathbf{q}}} + \widetilde{\mathbf{K}}\mathbf{L}\overline{\mathbf{q}} = \widetilde{\mathbf{f}} + \widetilde{\mathbf{g}} \\ \mathbf{L}^{T}\widetilde{\mathbf{g}} = \mathbf{0} \end{cases} \tag{19}$$

Finally, the assembled system can be obtained by premultiplying the equilibrium equations by $\mathbf{L}^{\mathrm{T}}$, which eliminates the connecting forces (i.e., $\mathbf{L}^{\mathrm{T}}\widetilde{\mathbf{g}} = \mathbf{0}$) as follows:

$$\overline{\mathbf{M}}\ddot{\overline{\mathbf{q}}} + \overline{\mathbf{K}}\overline{\mathbf{q}} = \overline{\mathbf{f}} \tag{20}$$

where,

$$\overline{\mathbf{M}} = \mathbf{L}^{\mathrm{T}}\widetilde{\mathbf{M}}\mathbf{L}, \overline{\mathbf{K}} = \mathbf{L}^{\mathrm{T}}\widetilde{\mathbf{K}}\mathbf{L}, \overline{\mathbf{f}} = \mathbf{L}^{\mathrm{T}}\widetilde{\mathbf{f}} \tag{21}$$

More details of the substructure assembly and general framework for dynamic substructuring are comprehensively documented in the work of Kleck and Rixen [4]. It is to be noted that the superscript (s) is explicitly shown only for this section to minimize notational clutter. To avoid confusion, it is explicitly mentioned when the global matrix is considered.

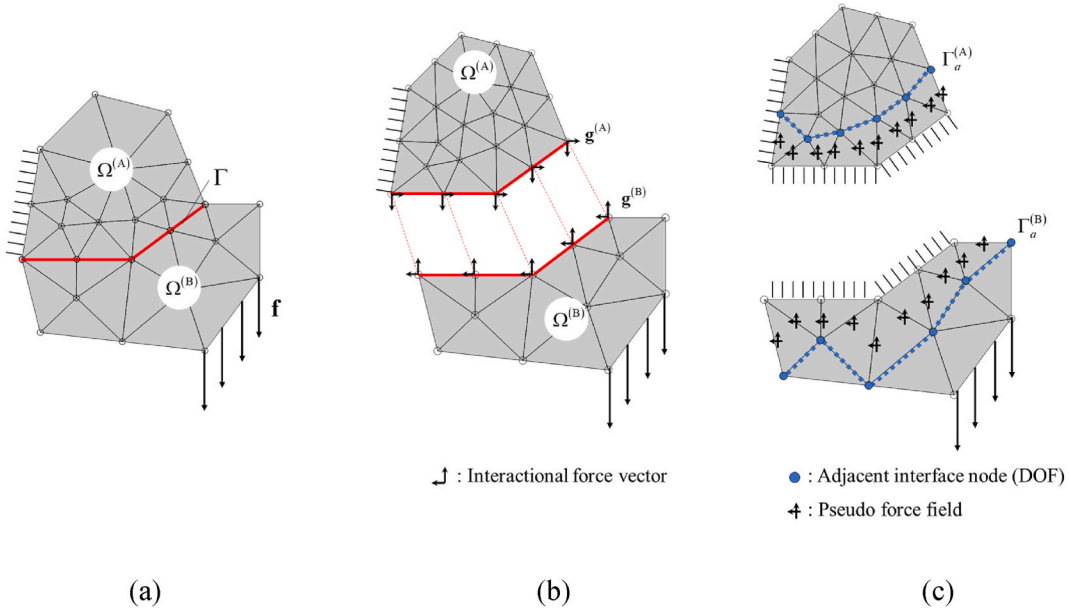

Fig. 2. Global and partitioned structural model and interface handling. (a) Global structure under an external force $\mathbf{f}$ in the global domain Ω and boundary Γ, (b) substructures in $\Omega^{(s)}(s = 1, 2, ..., N_s)$ and interactional forces $\mathbf{g}$, and (c) adjacent nodes in the adjacent boundary $\Gamma_a^{(s)}(s = 1, 2, ..., N_s)$ and the present pseudo-force approach.

2.3. Reduction method in general and our previous work

In general, three types of component modes are considered for a reasonable reduction basis: *rigid body*, *flexible,* and *static modes*. The first two modes, also called dynamic mode, account for the dynamic behavior of the substructure, whereas the last mode accounts for the interaction between neighboring substructures, ensuring that compatibility conditions after assembly are satisfied.

The approximated displacement can be written in the form of mode superposition:

$$\mathbf{u} = \mathbf{u}_{rigid} + \mathbf{u}_{flex} + \mathbf{u}_{stat} \tag{22}$$

where the rigid body, flexible, and static modes are denoted by the subscripts *rigid*.*flex*, and *stat*, respectively.

In 1968, Craig and Bampton developed the CB method. They utilized *internal vibration modes* and *constraint modes* as the flexible and static modes, respectively, in Eq. (22). The former, also called fixed interface eigenmodes, are obtained by solving the eigenvalue problem of the substructure fixed on its interface boundary, while the latter are defined as a unit displacement on one boundary DOF keeping all others fixed:

$$\left(\mathbf{K}_{ii} - \omega_{i,j}^2 \mathbf{M}_{ii}\right)\varphi_{i,j} = \mathbf{0}, \boldsymbol{\Phi}_i = [\varphi_1, \varphi_2, ...] \tag{23}$$

$$\boldsymbol{\Psi}_c = \begin{bmatrix} \boldsymbol{\Psi}_{c,i} \\ \boldsymbol{\Psi}_{c,b} \end{bmatrix} = \begin{bmatrix} -\mathbf{K}_{ii}^{-1}\mathbf{K}_{ib} \\ \mathbf{I} \end{bmatrix} \tag{24}$$

Here $\omega_{i,j}$ and $\varphi_{i,j}$ are the j^{th} eigenfrequency and associated eigenmode of the internal substructure, respectively, while a set of internal vibration modes and constraint modes are denoted by $\boldsymbol{\Phi}_i$ and $\boldsymbol{\Psi}_c$, respectively.

Realizing that rigid body motions are unnecessary if all boundary DOFs are included in the component modes and applying modal truncation to the set of internal vibration modes, Craig and Bampton presented the following approximate displacement:

$$\mathbf{u}_i = \mathbf{u}_{i.rigid} + \mathbf{u}_{i.flex} + \mathbf{u}_{i.stat} \approx \underbrace{\boldsymbol{\Phi}_i \boldsymbol{\eta}_i}_{flex} + \underbrace{\boldsymbol{\Psi}_{c,i}\mathbf{u}_b}_{stat\&rigid} \tag{25}$$

$$\begin{bmatrix} \mathbf{u}_i \\ \mathbf{u}_b \end{bmatrix} \approx \begin{bmatrix} \boldsymbol{\Phi}_i & \boldsymbol{\Psi}_{c,i} \\ \mathbf{0} & \mathbf{I} \end{bmatrix} \begin{bmatrix} \boldsymbol{\eta}_i \\ \mathbf{u}_b \end{bmatrix} = \mathbf{R}\mathbf{q} \tag{26}$$

where $\boldsymbol{\eta}_i$ represents the modal amplitudes corresponding to the mode shapes in $\boldsymbol{\Phi}_i$.

It is to be noted that the static constraint modes $\boldsymbol{\Psi}_{c,i}$ can be shifted to *quasi-static constraint modes* at a specific center-frequency as required [19]:

$$\boldsymbol{\Psi}_{c,i} = -\left(\mathbf{K}_{ii} - \omega_c^2 \mathbf{M}_{ii}\right)^{-1}\left(\mathbf{K}_{ib} - \omega_c^2 \mathbf{M}_{ib}\right) \tag{27}$$

where ω_c denotes the specific center frequency of interest. However, the quasi-static modes may still be insufficient for frequency analysis problems in the wideband domain because they can provide the displacement modes at only one center frequency.

While Craig and Bampton utilized unit displacement for static mode $\mathbf{u}_{stat}$, some researchers have attempted to utilize the unit force instead. This approach first appeared in the work of Rubin and Mac Neal, with a type of static mode called the attachment mode [16, 18]. Constraint modes are defined by specifying a unit displacement at one boundary DOF, while the others are fixed. Attachment modes are defined by specifying a unit force at one boundary DOF while letting the others free. Applying the unit force approach to the static modes in Eq. (22) yields the following approximation of the static modes:

$$\mathbf{u}_{stat} \approx \boldsymbol{\Psi}_a \mathbf{g}_b \tag{28}$$

$$\boldsymbol{\Psi}_a = \mathbf{K}^{+}\mathbf{F} \tag{29}$$

where the columns of the matrix $\boldsymbol{\Psi}_a$ contain individual attachment modes. $\mathbf{K}^{+}$ denotes the pseudo-inverse of the stiffness matrix, which is obtained by imposing imaginary constraints, called isostatic constraints, on some DOFs $\mathbf{u}_{ic}$. In other words, the pseudo-inverse matrix is:

$$\mathbf{K}^{+} = \begin{bmatrix} \mathbf{K}_{rm,rm}^{-1} & \mathbf{0} \\ \mathbf{0} & \mathbf{0} \end{bmatrix} \tag{30}$$

where the subscripts *ic* and *rm* denote the imaginary constraint DOFs and the remaining DOFs, except for the imaginary constraint. The columns of $\mathbf{F}$ impose a unit force on one boundary DOF:

$$\mathbf{F} = \begin{bmatrix} \mathbf{F}_i^{\mathrm{T}} & \mathbf{F}_b^{\mathrm{T}} \end{bmatrix}^{\mathrm{T}} = \begin{bmatrix} \mathbf{0} & \mathbf{I} \end{bmatrix}^{\mathrm{T}} \tag{31}$$

where $\mathbf{I}$ is the identity matrix acting on the boundary DOFs and $\mathbf{0}$ is a null matrix acting on the internal DOFs. Now the approximate displacement variable can be written with the reduction basis:

$$\mathbf{u} = \mathbf{u}_{rigid} + \mathbf{u}_{flex} + \mathbf{u}_{stat} \approx \underbrace{\boldsymbol{\Phi}_r \boldsymbol{\eta}_r}_{rigid} + \underbrace{\boldsymbol{\Phi}_f \boldsymbol{\eta}_f}_{flex} + \underbrace{\boldsymbol{\Psi}_a \mathbf{g}_b}_{stat} \tag{32}$$

where $\boldsymbol{\Phi}_r$, $\boldsymbol{\Phi}_f$ and $\boldsymbol{\eta}$ denote the rigid body, flexible mode and their corresponding modal amplitudes, respectively.

It is to be noted that subsequent procedures to obtain the strict attachment mode presented by Rubin and MacNeal are not described here. The unit force approach is easily implemented experimentally rather than numerically, compared to the unit displacement approach, because imposing imaginary constraints and calculating the optimal imaginary constraint set $\mathbf{u}_{ic}$ is non-intuitive and requires considerable computing time. In particular, for problems which require a new reduction system with each iteration, such as topology optimization and nonlinear problems, the computational time required to obtain the reduction basis and the accuracy of the approximation system both become significant.

Meanwhile, some studies have attempted to substitute the load-dependent Ritz vector (LDRV or simply RV) for the eigenmode of the substructures to utilize the advantages of LDRV, such as its accurate dynamic analysis and low computation cost [25–30]. However, the major problems with adopting the Ritz vector instead of the eigenmode for the substructuring scheme include the lack of external forces (loads) to initiate the Krylov sequence generating LDRV and the lack of proper boundary conditions for invertible dynamic stiffness matrices. Therefore, the computation of the LDRV for each substructure is not deterministic without external loads and boundary conditions.

To solve these problems, we introduced a certain force and boundary condition capable of initiating the subspace of the LDRV of a subsystem with no boundary and loading conditions. Instead of the imaginary boundary conditions explained in Eq. (30), we utilized interface boundary condition used in the general fixed interface methods and introduced the concept of the unit *pseudo-force* accordingly. The unit pseudo-force is defined as a set of unit forces applied to the DOFs of the *adjacent boundary*. Here the *adjacent boundary* Γ_a is defined as the set of remaining DOFs excluding the boundary DOFs among the domain of the finite elements containing the boundary interface Γ (see Fig. 2). The equations of motion in Eq. (10) can be written as following form by distinguishing the internal DOFs except for the adjacent boundary $\widehat{i}$, the adjacent boundary DOFs a, and the boundary DOFs b.

$$\mathbf{M} = \begin{bmatrix} \mathbf{M}_{\widehat{i}\widehat{i}} & \mathbf{M}_{\widehat{i}a} & \mathbf{0} \\ \mathbf{M}_{\widehat{i}a}^T & \mathbf{M}_{aa} & \mathbf{M}_{ab} \\ \mathbf{0} & \mathbf{M}_{ab}^T & \mathbf{M}_{bb} \end{bmatrix} \mathbf{K} = \begin{bmatrix} \mathbf{K}_{\widehat{i}\widehat{i}} & \mathbf{K}_{\widehat{i}a} & \mathbf{0} \\ \mathbf{K}_{\widehat{i}a}^T & \mathbf{K}_{aa} & \mathbf{K}_{ab} \\ \mathbf{0} & \mathbf{K}_{ab}^T & \mathbf{K}_{bb} \end{bmatrix} \mathbf{f} = \begin{bmatrix} \mathbf{f}_{\widehat{i}} \mathbf{f}_a \mathbf{f}_b \end{bmatrix} \mathbf{g} = \begin{bmatrix} \mathbf{g}_{\widehat{i}} \mathbf{g}_a \mathbf{g}_b \end{bmatrix} \tag{33}$$

In addition, a set of pseudo-forces $\mathbf{P}$ can be described by the following definition:

$$\mathbf{P} = \begin{bmatrix} \mathbf{P}_{\widehat{i}}^{\mathrm{T}} & \mathbf{P}_a^{\mathrm{T}} & \mathbf{P}_b^{\mathrm{T}} \end{bmatrix}^{\mathrm{T}} = \begin{bmatrix} \mathbf{0} & \mathbf{I} & \mathbf{0} \end{bmatrix}^{\mathrm{T}} \tag{34}$$

where $\mathbf{I}$ is the identity matrix acting on adjacent boundary DOFs, and $\mathbf{0}$ is a null matrix acting on the others. Now similar to the attachment mode in Eq. (29), *the pseudo-attachment mode* is defined by the quasi-static displacement (Ritz vectors) at a specific center-frequency ω_c with the unit pseudo-forces:

$$\boldsymbol{\Psi}_p = \mathbf{D}^{-1}\mathbf{P} \tag{35}$$

$$\mathbf{D}^{-1} = \left(\begin{bmatrix} \mathbf{K}_{ii} & \mathbf{0} \\ \mathbf{0} & \mathbf{0} \end{bmatrix} - \omega_c^2 \begin{bmatrix} \mathbf{M}_{ii} & \mathbf{0} \\ \mathbf{0} & \mathbf{0} \end{bmatrix} \right)^{-1} \tag{36}$$

Here the columns of the matrix $\boldsymbol{\Psi}_p$ contain individual pseudo-attachment modes. To describe our previous approach more intuitively, the matrix of pseudo-attachment modes $\boldsymbol{\Psi}_p$ is described as if quasi-static displacements at single center frequency in here. However, it is obtained by the Ritz vector method for the multi-frequency multi-load case (detailed procedures to calculate Ritz vectors with multi-loads at multi-center frequencies will be discussed in the next section). The shape of the pseudo-attachment modes has intriguing characteristics with both internal vibration (flexible) and constraint mode shapes (see Appendix 1 for more detailed characteristics of Ritz vectors generated by the unit pseudo-force).

Substituting the internal vibration modes with the Ritz vectors obtained by globally imposed external forces and boundary conditions and adding this pseudo-attachment mode to the static modes leads to the following approximation of the displacement vector:

$$\mathbf{u} = \mathbf{u}_{rigid} + \mathbf{u}_{flex} + \mathbf{u}_{stat} = \underbrace{\boldsymbol{\Phi}_R \boldsymbol{\eta}_R}_{flex} + \underbrace{\boldsymbol{\Psi}_p \mathbf{g}_a}_{flex,quasi-stat} + \underbrace{\boldsymbol{\Psi}_c \mathbf{u}_b}_{rigid,stat} \tag{37}$$

where $\boldsymbol{\Phi}_R$ and $\boldsymbol{\eta}_R$ represent the Ritz vectors (or assumed mode) obtained by external force and boundary condition and their corresponding modal amplitude, respectively. The inclusion of the non-reduced DOFs, $\mathbf{u}_b$, and the expression in Eq. (5), yielded the following reduction basis:

$$\begin{bmatrix} \mathbf{u}_i \\ \mathbf{u}_b \end{bmatrix} \approx \begin{bmatrix} \boldsymbol{\Phi}_{R,i} & \boldsymbol{\Psi}_p & \boldsymbol{\Psi}_{c,i} \\ \mathbf{0} & \mathbf{0} & \mathbf{I} \end{bmatrix} \begin{bmatrix} \boldsymbol{\eta}_{R,i} \\ \mathbf{g}_a \\ \mathbf{u}_b \end{bmatrix} = \mathbf{R}\mathbf{q} \tag{38}$$

This Ritz vector-based substructuring was named the multi-component quasi-static Ritz vector (MQSRV) method [32].

3. Interface eigenmode based-MQSRV (IMQSRV) method

The MQSRV method improves the accuracy of the approximated model by substituting the eigenmodes of the conventional method with Ritz vectors and adding multiple quasi-static modes that account for the interaction between neighboring substructures in a quasi-static state. However, the number of pseudo-attachment modes in the MQSRV method cannot be reduced, just as the number of constraint modes in the CB method is equal to the number of boundary DOFs, even larger than the number of (adjacent) interface boundary DOFs because its column comprises multiple quasi-static modes. This dependency results in the inevitable large size of the reduction matrix **R**.

To resolve this issue, the concept of generalized pseudo-forces is proposed for the effective reduction of the basis:

$$\mathbf{P}_a = \mathbf{I} \in \mathbb{R}^{a\times a} \tag{39}$$

$$\widetilde{\mathbf{P}}_a \in \mathbb{R}^{a\times d}, d < a \tag{40}$$

where $\widetilde{\mathbf{P}}_a$ is an approximated pseudo-force matrix containing d individual generalized pseudo-forces. The approximated pseudo-force space should be the subspace of the vector space spanned by the unit force vectors and be fully recoverable to the unit force vector space. In order to find a subspace that satisfies the above condition, we first transform the adjacent interface displacement to mode superposition form. By solving the eigenproblem of the pseudo interface equations, the adjacent interface displacement modes and adjacent displacement eigenfrequencies are obtained:

$$\left[\mathbf{K}_{aa} - \omega_{a,j}^2 \mathbf{M}_{aa}\right]\varphi_{a,j}^* = 0 \tag{41}$$

Now the response in adjacent interface DOFs can be written as mode superposition form:

$$\mathbf{u}_a = \sum_{j=1}^{n_a} \varphi_{a,j}\eta_{a,j} \tag{42}$$

Just as unit displacement approach is converted to unit force approach as introduced in section 2, the obtained adjacent

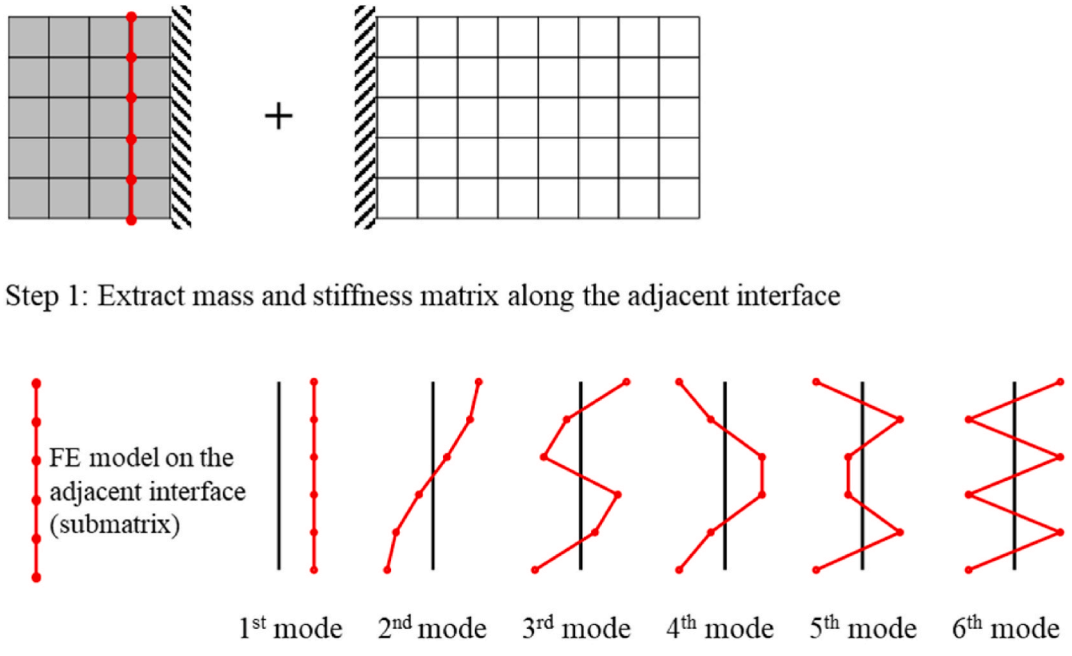

Fig. 3. Schematic of the generation of Ritz vectors with the eigenmode-shape pseudo-forces.

displacement is converted to the adjacent force through the following normalizing process:

$$\text{Normalization}: \varphi_{a,j} = \frac{1}{\sqrt{\varphi_{a,j}^{*\,\mathrm{T}} \cdot \varphi_{a,j}^{*}}} \varphi_{a,j}^{*} \tag{43}$$

By selecting d lowest eigenmodes in low order, the eigenmode-shape pseudo-forces can effectively transfer the energy between the substructures compared to other possible pseudo-forces and be easily recovered to the vector space spanned by unit pseudo-forces by selecting all eigenmodes of the adjacent interface:

$$\mathbf{\Pi}_a = [\varphi_1, \varphi_2, ..., \varphi_{n_a}] \tag{44}$$

$$\mathbf{\Pi}_{a,d} = [\varphi_1, \varphi_2, ..., \varphi_d], (d < n_a) \tag{45}$$

Here n_a is the number of adjacent DOFs, which is equal to the number of unit pseudo-forces. Based on the above idea, it is possible to employ distributed loads whose shapes resemble those of the eigenmodes along the adjacent interface (the so-called *eigenmode-shape pseudo-force*), as shown in Fig. 1(b) and Fig. 3.

Now a set of eigenmode-shape pseudo-forces can be described by the following definition:

$$\widetilde{\mathbf{P}} = \begin{bmatrix} \widetilde{\mathbf{P}}_i^{\mathrm{T}} & \widetilde{\mathbf{P}}_a^{\mathrm{T}} & \widetilde{\mathbf{P}}_b^{\mathrm{T}} \end{bmatrix}^{\mathrm{T}} = \begin{bmatrix} \mathbf{0} & \mathbf{\Pi}_{a,d}^{\mathrm{T}} & \mathbf{0} \end{bmatrix}^{\mathrm{T}} = [\widetilde{p}_1, ..., \widetilde{p}_j, ..., \widetilde{p}_d] \tag{46}$$

where $\widetilde{p}_j$ is a j^{th} eigenmode-shape pseudo-force stored in the columns of matrix $\widetilde{\mathbf{P}}$.

A block Ritz vector algorithm is utilized to generate orthogonal bases for obtaining the LDRV for multiple loads (forces) and multiple-center frequencies. The block Ritz vector method creates a block of Ritz vectors for different load vectors at each step, which imposes orthogonalization both among the blocks and the different Ritz vectors in each block (references [25,34] provide more details about the block orthogonalization process). For exposition, we assume that there are two eigenmode-shape pseudo-forces, $\widetilde{p}_1$ and $\widetilde{p}_2$ with a single center frequency ω_c. Then, the block Ritz vector algorithm can be described as follows.

For block number $i = 1$

$$\psi_{1,k}^{*} = \left(\mathbf{K} - \omega_c^2 \mathbf{M}\right)^{-1} \widetilde{p}_k \ (k = 1, 2) \tag{47}$$

$$\psi_{1,1} = \frac{\psi_{1,1}^{*}}{\left(\psi_{1,1}^{*\,T} \mathbf{M} \psi_{1,1}^{*}\right)^{1/2}} \quad \text{(Normalization)} \tag{48}$$

$$\psi_{1,2}^{**} = \psi_{1,2}^{*} - \left(\psi_{1,1}^{*} \mathbf{M} \psi_{1,2}^{*}\right) \psi_{1,1}^{*} \ \text{(Orthogonalization } \textit{in} \text{ the each block)} \tag{49}$$

$$\psi_{1,2} = \frac{\psi_{1,1}^{**}}{\left(\psi_{1,2}^{**\,\mathrm{T}} \mathbf{M} \psi_{1,2}^{**}\right)^{1/2}} \quad \text{(Normalization)} \tag{50}$$

For block numbers $i = 2, 3, ..., n_{Kry}$

$$\psi_{i,k}^{*} = \left(\mathbf{K} - \omega_c^2 \mathbf{M}\right)^{-1} \mathbf{M} \, \psi_{i-1,k} \ (k = 1, 2) \tag{51}$$

$$\psi_{i,1}^{**} = \psi_{i,1}^{*} - \sum_{j=1}^{i-1} \left(\psi_{j,1}^{\mathrm{T}} \mathbf{M} \psi_{i,1}^{*}\right) \psi_{j,1} - \sum_{j=1}^{i-1} \left(\psi_{j,2}^{\mathrm{T}} \mathbf{M} \psi_{i,1}^{*}\right) \psi_{j,2} \tag{52}$$

(Orthogonalization *among* the previous blocks)

$$\psi_{i,1} = \frac{\psi_{i,1}^{**}}{\left(\psi_{i,1}^{**\,\mathrm{T}} \mathbf{M} \psi_{i,1}^{**}\right)^{1/2}} \quad \text{(Normalization)} \tag{53}$$

$$\psi_{i,2}^{**} = \psi_{i,2}^{*} - \sum_{j=1}^{i-1} \left(\psi_{j,1}^{\mathrm{T}} \mathbf{M} \psi_{i,2}^{*}\right) \psi_{j,1} - \sum_{j=1}^{i-1} \left(\psi_{j,2}^{\mathrm{T}} \mathbf{M} \psi_{i,2}^{*}\right) \psi_{j,2} \tag{54}$$

(Orthogonalization *among* the previous blocks)

$$\psi_{i,2} = \frac{\psi_{i,2}^{**}}{\left(\psi_{i,2}^{**\,\mathrm{T}} \mathbf{M} \psi_{i,2}^{**}\right)^{1/2}} \quad \text{(Normalization)} \tag{55}$$

where n_{Kry} is the number of Krylov sequences used to generate the Ritz vectors.

Now, a matrix containing each Ritz vector by two eigenmode-shape pseudo-forces at a single center frequency ω_c is described as

follows:

$$\boldsymbol{\Psi}_{\omega_c} = \left[\overbrace{\{\psi_{1,1}, \cdots, \psi_{n_{Kry},1}\}}^{\text{Ritz vector block for } \tilde{p}_1}, \overbrace{\{\psi_{1,2}, \cdots, \psi_{n_{Kry},2}\}}^{\text{Ritz vector block for } \tilde{p}_2} \right] \tag{56}$$

Then, the Ritz vectors at the single center frequency ω_c can be extended with multiple center frequencies by the same block orthogonalization process in Eqs. 47–55. The approximated pseudo-attachment modes calculated by the Krylov sequence initiated by eigenmode-shape pseudo-forces and muti-center frequencies can be defined as follows:

$$\widetilde{\boldsymbol{\Psi}}_p = \left[\boldsymbol{\Psi}_{\omega_{c1}}, \ldots, \boldsymbol{\Psi}_{\omega_{cj}}, \ldots, \boldsymbol{\Psi}_{\omega_{cn_c}} \right] \tag{57}$$

where ω_{cj} is the j th center frequency out of n_c. And the Ritz vectors computed at all the center frequencies are stored in columns of the matrix $\widetilde{\boldsymbol{\Psi}}_p$. Finally, we present the following approximated displacement and reduction matrix:

$$\mathbf{u} = \mathbf{u}_{rigid} + \mathbf{u}_{flex} + \mathbf{u}_{stat} = \underbrace{\boldsymbol{\Phi}_R \boldsymbol{\eta}_R}_{flex} + \underbrace{\widetilde{\boldsymbol{\Psi}}_p \boldsymbol{\eta}_p}_{flex,quasi-stat} + \underbrace{\boldsymbol{\Psi}_c \mathbf{u}_b}_{rigid,stat} \tag{58}$$

$$\begin{bmatrix} \mathbf{u}_i \\ \mathbf{u}_b \end{bmatrix} \approx \begin{bmatrix} \boldsymbol{\Phi}_{R,i} & \widetilde{\boldsymbol{\Psi}}_{p,i} \boldsymbol{\eta}_{p,i} & \boldsymbol{\Psi}_{c,i} \\ \mathbf{0} & \mathbf{0} & \mathbf{I} \end{bmatrix} \begin{bmatrix} \boldsymbol{\eta}_{R,i} \\ \boldsymbol{\eta}_{p,i} \\ \mathbf{u}_b \end{bmatrix} = \mathbf{R}\mathbf{q} \tag{59}$$

where $\boldsymbol{\eta}_{p,i}$ represents the approximated force amplitudes corresponding to the interior Ritz vectors obtained by eigenmode-shape pseudo-forces $\widetilde{\boldsymbol{\Psi}}_{p,i}$.

This approach is called the interface eigenmode-based MQSRV (IMQSRV) method to distinguish from the previous MQSRV method. The following remarks on the reduction matrices in (38) and (59) are noteworthy.

- In the present MQSRV and IMQSRV methods, where the (quasi-) static response of the reduced DOFs is determined by pseudo-attachment modes in addition to the constraint modes discussed in Eq. (24), the dynamic response is approximated by the Ritz vectors computed with globally defined forces (external loads) along with the pseudo-forces defined in Eqs. (39) and (40). However, the dynamic response of the Ritz vectors may be accounted for twice, especially when the external forces act on the adjacent interface DOFs. This could be the cause of the singularity problem. Therefore, Ritz vectors obtained by the external and pseudo-forces are orthogonalized to each other by the block orthogonalization process in Eqs. 47–55.
- The quasi-static constraint modes in Eq. (27) and pseudo-attachment modes in Eq. (35), which are obtained at the same center frequency, can be considered to have similar mode shapes. This is disadvantageous for convergence and efficiency reasons, although no singularity issue arises because these modes are not exactly the same. Therefore, different center frequencies are recommended for the pseudo-attachment modes and quasi-static constraint modes.
- Because the IMQSRV method addresses reduction basis obtained by the Ritz vector method and not the reduction of the interface DOFs, it is unaffected by coupled or uncoupled interfaces [3,11,14,21].
- In modal-based model order reduction techniques, both eigenmode-based and Ritz vector-based methods utilize additional process to distinguish between modes of interest and unnecessary modes including spurious modes. Eigenmode-based approaches generally utilize a process called frequency cut-off [8,24], which aids in selecting the modes of interest while discarding unnecessary ones. Similarly, Ritz vector-based order reduction methods utilize a vector termination algorithm to determine the required number of Ritz vectors for a given problem [25]. However, it is noted that the above termination algorithm is not used in this paper because only the minimum Ritz vector is used to facilitate direct comparison with the conventional methods.

4. Numerical examples

In this section, we examine the performance of the MQSRV and IMQSRV methods compared to the conventional CMS method (i.e., CB) as a reference. Since the (approximated) pseudo-attachment modes are obtained at multiple center frequencies, the MQSRV and IMQSRV methods generally require more DOFs in reduced models that possess a large number of boundary DOFs than the conventional CB method. Therefore, the number of dominant modes for the CB method was determined based on the size of the reduced model using the IMQSRV method rather than the frequency cutoff mode selection technique.

Two different structural models discretized by different finite elements are considered: a cantilever beam with four-node quadrilateral and three-node triangular element and 3D solid pipe with eight-node hexahedral and four-node mixed interpolation of tensorial components (MITC) shell elements. The numerical examples are solved with the multi-frontal solver in MATLAB (Matlab 2016b, 64bit, i7-4770 4 cores, 32 GB).

The relative eigenvalue error is usually used to evaluate the performance of the CMS methods. However, this error based on the eigenfrequency analysis is unsuitable for evaluating the proposed method because it is not based on the actual eigenmodes. Therefore, the following force-normalized relative response error based on frequency response analysis is used to evaluate the performance of the IMQSRV method:

$$\text{LogError} = \log_{10}\left(\frac{\left|\left|\mathbf{f}^{\mathrm{T}}\mathbf{u}\right|/|\mathbf{f}| - \left|\mathbf{f}^{\mathrm{T}}\tilde{\mathbf{u}}\right|/|\mathbf{f}|\right|}{\left|\mathbf{f}^{\mathrm{T}}\mathbf{u}\right|/|\mathbf{f}|}\right) \tag{60}$$

where $\mathbf{u}$ and $\tilde{\mathbf{u}}$ denote the displacements at a specific frequency obtained by the full order model (FOM) and reduced order model (ROM), respectively.

4.1. Rectangular plate problem

Let us consider a rectangular plate with the boundary conditions shown in Fig. 4. Its length, width, and thickness are 0.6 *m*, 0.3 *m*, and 0.01 *m*, respectively. The model is partitioned into two substructures ($N_s = 2$) with arbitrarily determined material properties, namely, the Young's modulus E, Poisson's ratio ν, and density ρ are 1 Pa, 0.3, and $1\mathrm{kg/m^3}$, respectively. The plate was modeled by 15×8 four-node MITC shell FEs.

In this example, two different frequency domains are considered: range1 lies between 0 and 10 (rad/s), while range2 is from 20 to 25 (rad/s), and the number of frequency steps is 500. For frequency range1, we consider three numerical cases with 5, 20, and 40 (all) eigenmode-shape pseudo-forces. The center frequency and number of Krylov subspaces are set to [0, 5, 10] (rad/s) and one, respectively. Meanwhile, 15, 60, and 120 dominant substructural eigenmodes of the CB method were selected for comparison. The sizes of the reduced-order model (ROM) by the CB method obtained by each dominant eigenmode were 70, 160, and 280. The IMQSRV method has three more bases that are calculated by external forces at each center frequency. The numbers of retained modes for each method and the computation time for calculating the reduction basis are listed in Table 1, which demonstrates that the IMQSRV method uses less computational resources to calculate the reduction basis because it does not require the modal analysis of the entire system. On the other hand, given that the computational cost for calculating the basis is relatively small compared to the total frequency analysis time, it becomes evident that the overall computational cost (as seen in Table 1, demonstrating the speed-up effect) is comparable to that of the CB and IMQSRV methods. Fig. 5 presents the force-normalized frequency responses and their error curves. The results show that the IMQSRV method outperforms the CB method around the center frequencies when the same number of bases is used. While the CB method shows better performance around natural (eigen) frequencies, the performance of the IMQSRV method deteriorates slightly around natural frequencies because exact eigenmodes are not used.

For frequency range2, the center frequencies [20, 22.5, 25] (rad/s) are used instead of [0, 5, 10] (rad/s). All the other numerical conditions were maintained. Fig. 6 shows the advantage of the IMQSRV method, which maintains its performance without additional calculations to select proper eigenmodes depending on the frequency domain. The numbers of retained modes and computation time for frequency range2 are listed in Table 2.

4.2. Cantilever beam problem

We consider a cantilever beam, as shown in Fig. 7, whose left side is clamped, and the other side is subjected to a unit load. The beam is modeled by two different FEs: one is a 16×4 four-node quadrilateral (quad) FE and the other is a randomly discretized three-node triangular FE. The model is partitioned into four substructures ($N_s = 4$), with arbitrarily-determined material properties: the Young's modulus E is 100 Pa, Poisson's ratio ν is 0.3, and density ρ is $1\mathrm{kg/m^3}$ for the hard material ($\Omega^{(1)}$ and $\Omega^{(3)}$), while the Young's modulus E is 1 Pa, Poisson's ratio ν is 0.3, and density ρ is $1\mathrm{kg/m^3}$ for a soft material ($\Omega^{(2)}$ and $\Omega^{(4)}$). Finally, the frequency analysis domain was set from 0 to 20 rad/s with 500 frequency steps.

We consider three numerical cases with different center frequencies. The number of eigenmode-shape pseudo-forces and number of Krylov subspaces are six and one, respectively. The center frequency ranges are: center frequency range 1: [0, 2.5, 5] (rad/s), center frequency range 2: [7.5, 10, 12.5]) (rad/s), and center frequency range 3: [15, 17.5, 20] (rad/s). Each center frequency range is denoted as R1, R2, and R3 in the following figures. For comparison, 20 dominant substructural modes were selected for the CB method. Fig. 8 presents the frequency responses and corresponding LogError values obtained by the IMQSRV method compared with those of

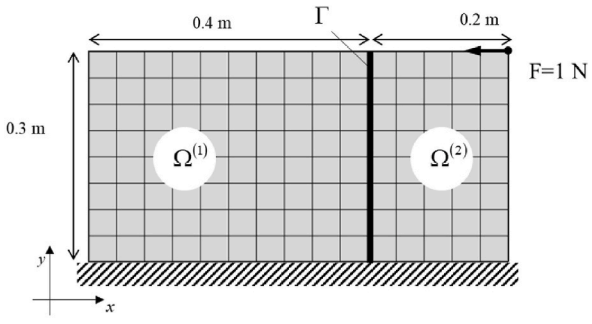

Fig. 4. Rectangular plate problem.

Table 1
Numbers of retained modes for each method and the computation time for calculating the reduction basis for the low-frequency case of example 4.1 (Frequency range 1: 0–10 (rad/s)).

Method	Number of eigenmode-shape pseudo forces n_p or, dominant substructural modes n_d	Size of Model	Base generation CPU time (s)	Speed up (Analysis time of FOM/ ROM)
IMQSRV	5	73	0.0418	114.02
	20	163	0.0416	23.54
	40 (max)	283	0.0425	10.30
CB	15	70	0.1783	103.62
	60	160	0.1791	23.12
	120	280	0.1755	11.92

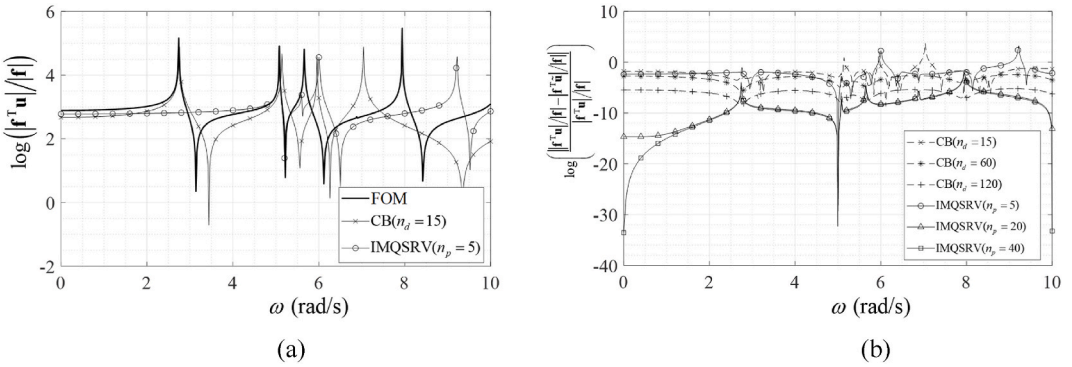

Fig. 5. (A) Frequency responses and (b) their error curves based on the CB and IMQSRV methods in range 1 (The number of dominant substructural eigenmodes and eigenmode-shape pseudo-forces is denoted by n_p and n_d).

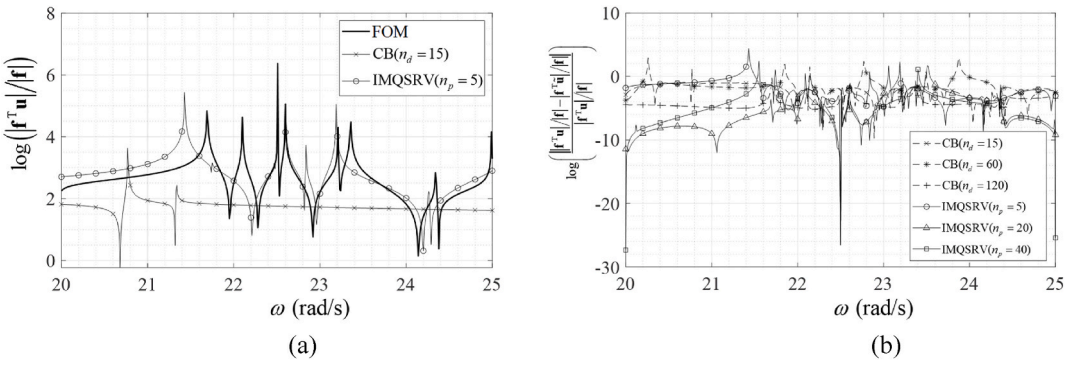

Fig. 6. (A) Frequency response and (b) their error curves based on the CB and IMQSRV methods in range 2.

Table 2
Numbers of retained modes for each method and the computation time for calculating the reduction basis for the high-frequency case of example 4.1 (Frequency range 2: 20–25 (rad/s)).

Method	Number of eigenmode-shape pseudo forces n_p or, dominant substructural modes n_d	Size of Model	Base generation CPU time (s)	Speed up (Analysis time of FOM/ ROM)
IMQSRV	5	73	0.0412	99.6
	20	163	0.0391	23.82
	40 (max)	283	0.0821	11.55
CB	15	70	0.1775	88.11
	60	160	0.1768	23.12
	120	280	0.1845	9.83

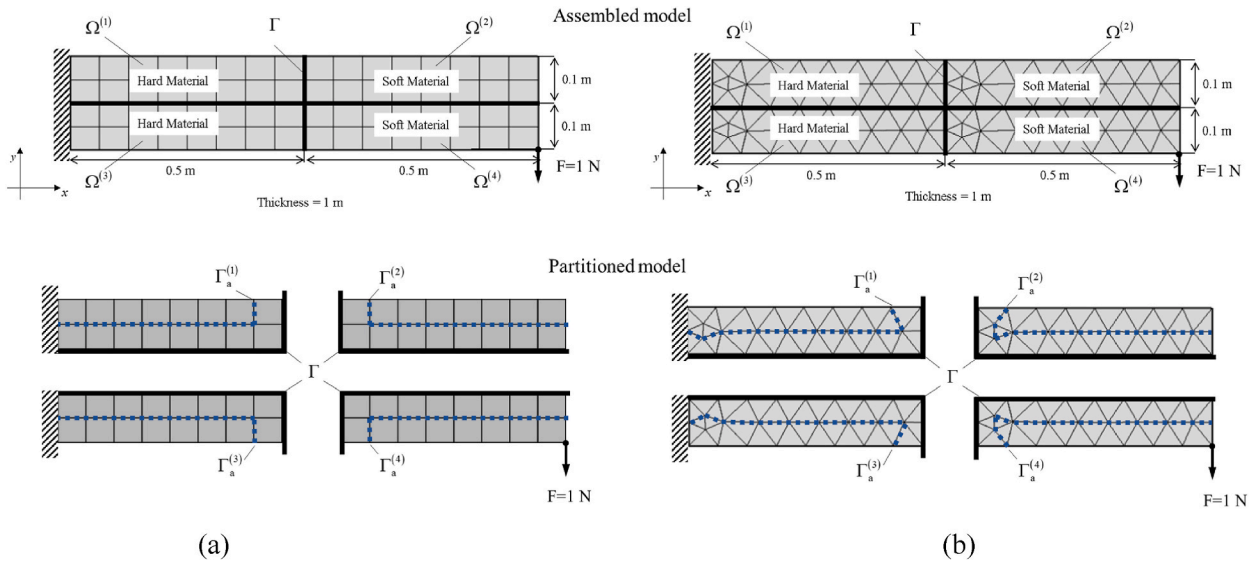

Fig. 7. Cantilever beam problem with different FEs. Four-node quadrilateral FEs (a) and three-node triangular FEs (b).

the CB method. The results demonstrate a characteristic feature of the present method, namely, the accuracy increases around the center frequencies, while accuracy of the CB method remains relatively constant. In addition, it can be confirmed that similar performance can be achieved regardless of the type of FE.

Next, we consider three numerical cases in the four-node quad FE model with 3, 5, and 54 (Max) eigenmode-shape pseudo-forces selected compared to the MQSRV method. For both the IMQSRV and MQSRV methods, the center frequency and number of Krylov subspaces were set to [0, 10, 20](rad/s) and one, respectively. As discussed in Section 3, Fig. 9 shows that the same performance can be obtained with the MQSRV method when all eigenmode-shape pseudo-forces are used. Although the MQSRV method can exhibit robust performance, it is limited by the size of the ROM exceeding that of the full order (original) model. (In this problem with quad element, the size of FOM is 170 while the size of ROM using the MQSRV meth.

4.3. 3D solid pipe problem

In the next example, we consider a 3D solid pipe problem (Fig. 10). The height H, radius R, and thickness t are 2 m, 1 m, and 0.5 m, respectively, while the Young's modulus E, Poisson's ratio ν, and density ρ are arbitrarily set to 100 Pa,0.3, and $1\mathrm{kg/m^3}$, respectively. The pipe structure partitioned into four substructures ($N_s = 4$) was modeled by two different FEs: one with a mesh of 32 (circumferential) $\times$ 3 (radial)$\times$ 10 (axial) brick elements (10) and once by a mesh of 32 (circumferential)$\times$ 10 (axial) MITC shell elements (Fig. 11). The left side of the pipe was clamped, and shear stress of -1 Pa was applied on the right side along the z-direction. Finally, the frequency analysis domain was set from 0 rad/s to 2 rad/s with 500 frequency steps.

For the brick element model, we assigned one Krylov subspace and three center frequencies: [0, 2.5, 5] (rad/s) for the IMQSRV and MQSRV methods. From each substructure, ten eigenmode-shape pseudo-forces and thirty dominant substructural eigenmodes were selected for the IMQSRV and CB methods, respectively. The size of the FOM was 4224, while the sizes of the ROM with the CB, IMQSRV, and MQSRV methods were 600, 612, and 3708, respectively. For the MITC shell element model, we applied the same numerical conditions, and the corresponding sizes of the FOM and ROM with the CB, IMQSRV, and MQSRV methods were 2112, 320, 332, and 1412, respectively.

The results of FRA and the corresponding error curves, plotted in Figs. 12 and 13, consistently demonstrate the robustness and efficiency of the IMQSRV method for the different type of finite element. The detail results for each case are summarized in Table 3 and 4.

5. Conclusions

This study presents a new substructuring method called the IMQSRV method, which is based on quasi-static LDRVs for both dynamic and static modes. In our previous substructuring method, the unit pseudo-force and pseudo-attachment mode approach, employed to construct a set of reduction bases (shown in Fig. 1(a)). Consequently, the large number of bases involved in the substructuring method becomes an issue for complex interfaces. To compute the LDRVs for multiple components efficiently considering interfaces, the *eigenmode-shape pseudo-force* concept based on the energy transfer approach, as shown in Fig. 1(b), is presented here. Thus, the number of LDRVs required for the pseudo-attachment mode can be reduced. Several numerical examples illustrate the characteristics of the present method that yields significantly more accurate frequency responses with less computation cost compared

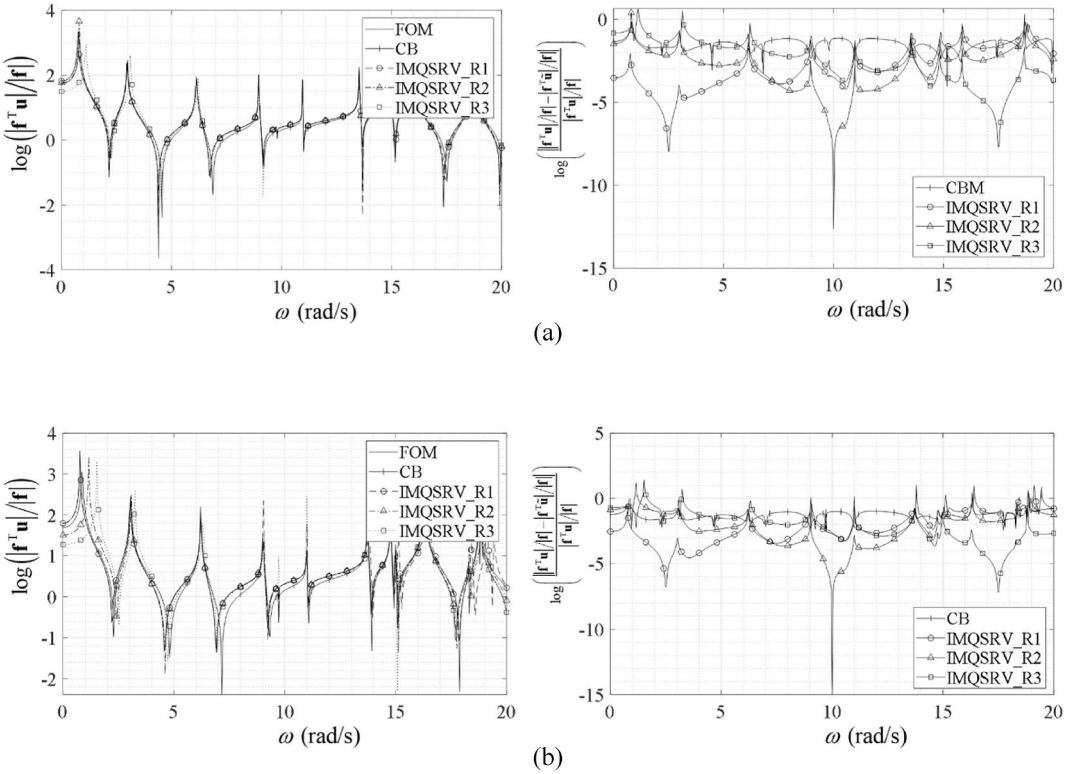

Fig. 8. Comparison of the frequency response and their error curves with different center frequencies. (a) Four-node quadrilateral FEs and (b) three-node triangular FEs.

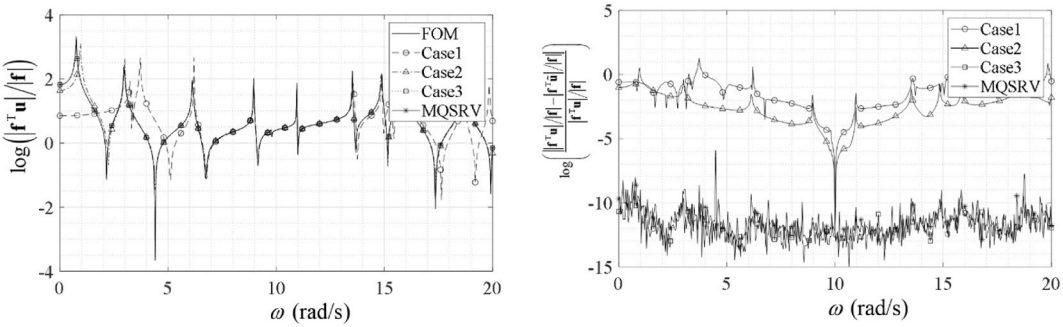

Fig. 9. Frequency response and their error curves with respect to different methods and different number of eigenmode-shape pseudo-forces (case 1: $n_p = 3$, case 2: $n_p = 5$, and case 3: $n_p = 54(\max)$).

to the conventional eigenmode-based substructuring method. The computational cost can be dramatically reduced by selecting an appropriate number of eigenmode-shape pseudo-forces, especially for complex interface problems. However, we could not find a meaningful way to select an appropriate number of eigenmode-shape pseudo-forces in general cases. This will be the subject of future research. In addition, the proposed approach is expected to be applicable to structural optimization problems that require iterative simulations by utilizing the less computational time required to generate a reduction basis.

Author's novelty

This study presents a new substructuring method based on the quasi-static Ritz vector method; This study presents a concept of pseudo attachment modes which are obtained by unit forces applied on adjacent interface degrees of freedom (DOFs); This study presents a concept of eigenmode-shape pseudo forces which are based on the eigenmode shapes of interface to reduce the number of interface DOFs.

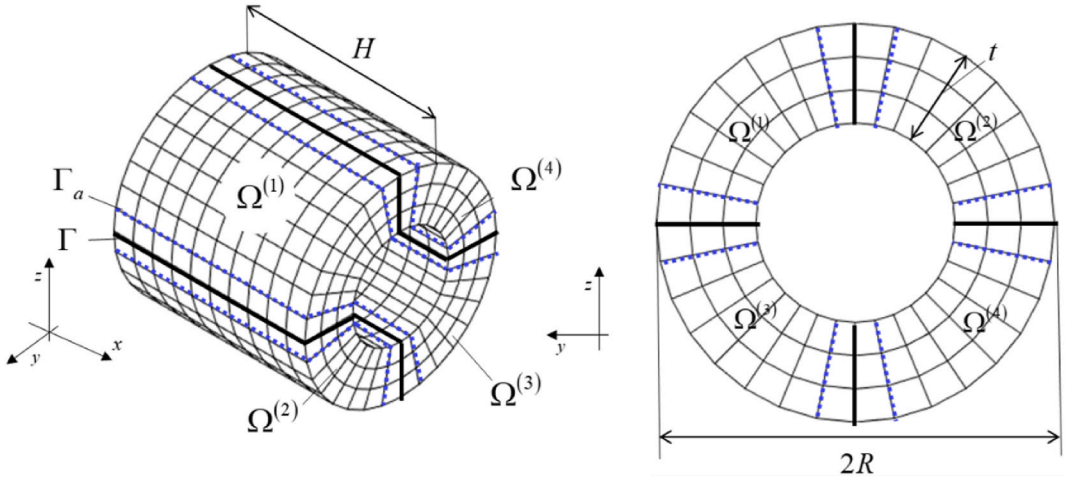

Fig. 10. 3D solid pipe problem with the eight-node hexahedral (brick) FEs.

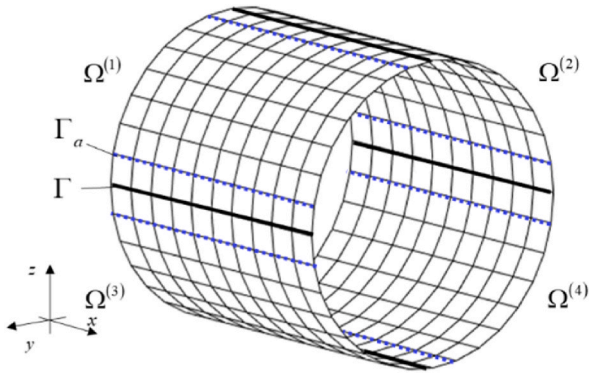

Fig. 11. 3D solid pipe problem with the four-node MITC shell FEs.

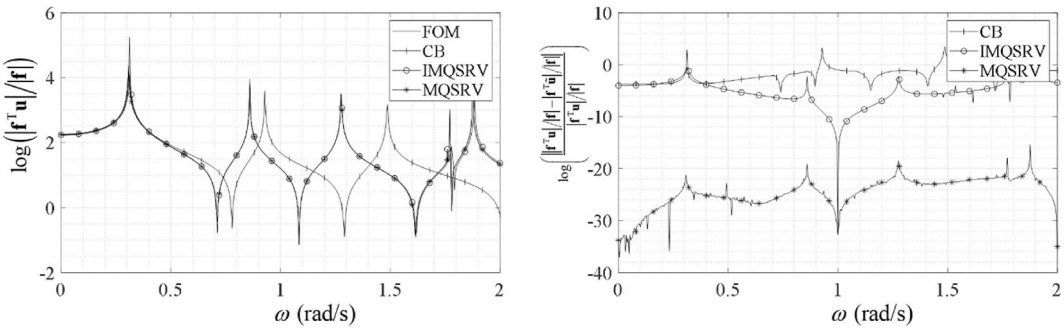

Fig. 12. Comparison of the frequency response and error curves with respect to the CB, MQSRV, and IMQSRV methods. The model was discretized using brick elements.

Declaration of competing interest

On behalf of all authors, the corresponding author states that there is no conflict of interest.

Data availability

Data will be made available on request.

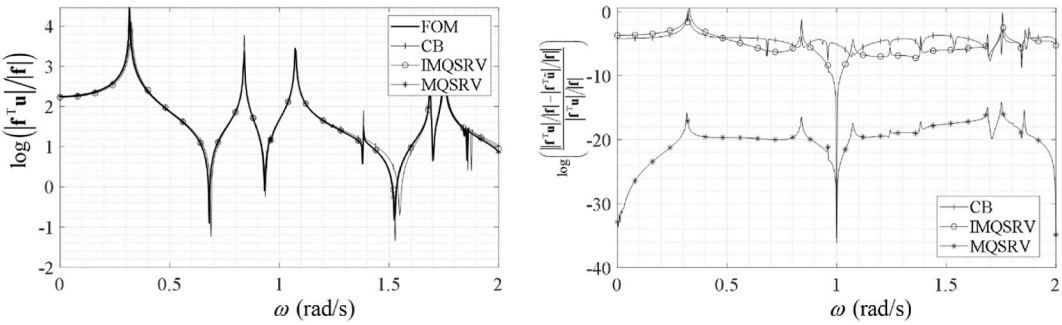

Fig. 13. Comparison of the frequency response and their error curves with respect to the CB, MQSRV, and IMQSRV methods. The model was discretized using MITC shell elements.

Table 3
Numbers of retained modes for each method and the computation time for calculating the reduction basis for the brick element case of example 4.3.

Method	Number of eigenmode-shape pseudo forces, n_p or, dominant substructural modes, n_d	Size of Model	Base generation CPU time (s)
CB	10	600	19.96
IMQSRV	30	612	2.32
MQSRV	264	3708	20.89

Table 4
Numbers of retained modes for each method and the computation time for calculating the reduction basis for shell element case of example 4.3.

Method	Number of eigenmode-shape pseudo forces, n_p or, dominant substructural modes, n_d	Size of Model	Base generation CPU time (s)
CB	10	320	0.81
IMQSRV	30	332	0.21
MQSRV	100	1412	1.02

Acknowledgements

This work was supported by the National Research Foundation of Korea (NRF) grant funded by the Korea government (MSIT) (NRF-2019R1A2C2084974).

Appendix 1. Characteristic of Ritz vector with point wise pseudo-forces

The constraint modes of the CB method in Eq. (26) are derived from Guyan's condensation method [9,10]. These modes account for the contribution of the boundary interface coordinate by unit displacement at all degrees of freedom of the boundary interface. Instead of *unit displacements*, we propose using *unit forces* that can be applied to all the coordinates of the adjacent boundary interface to generate LDRVs, which are called *pseudo-attachment modes*. Some intriguing mode shapes are observed. Figure A1 (a) and (b) show the eigenmode and constraint mode shapes of the half component of the 1 m × 0.1 m free-free plate, while (c) shows the shape of the pseudo-attachment modes of our previous method. As shown in Figure A1 (c), the pseudo-attachment modes generated by *the unit pseudo-force* exhibit the characteristics of both dynamic and static modes. Thus, the MQSRV method may yield both dynamic and static modes of the CB method through a single LDRV calculation.

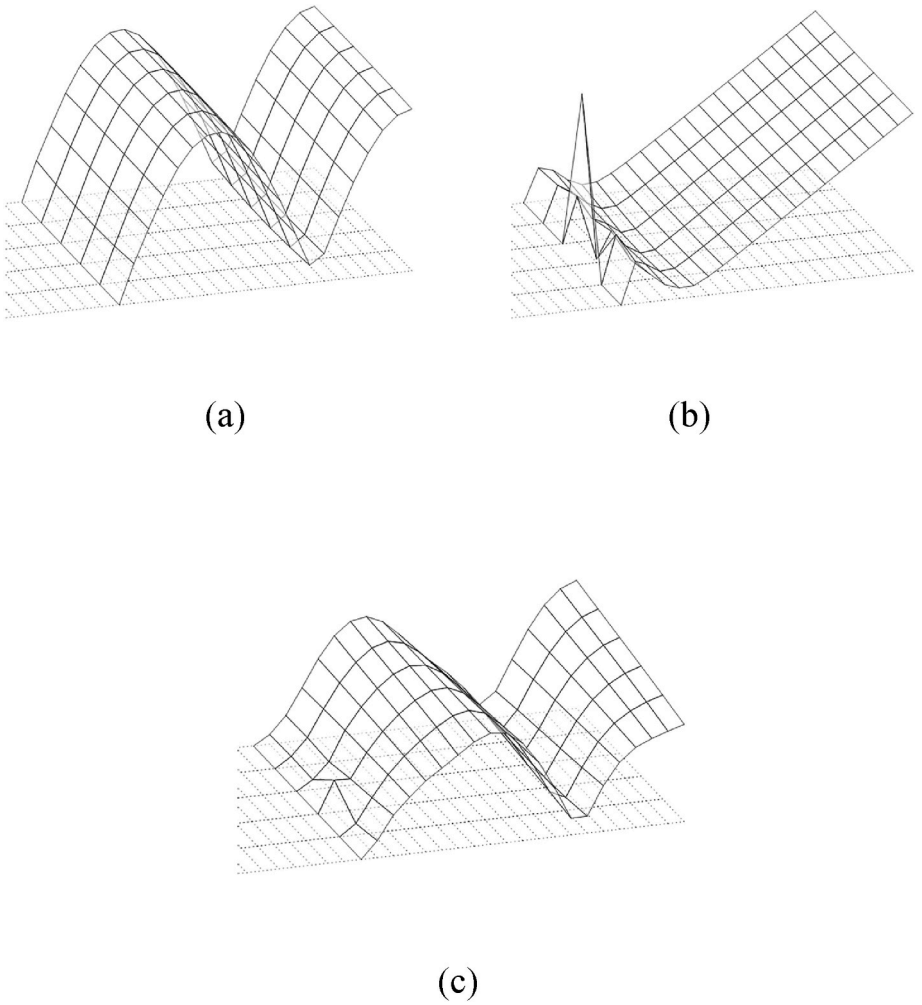

Fig. A1. Shapes of the substructural modes. Shapes of the (a) eigenmode of CB method, (b) constraint mode of CB method, and (c) pseudo attachment mode of MQSRV method.

References

[1] R.R. Craig Jr., C.-J. Chang, On the use of attachment modes in substructure coupling for dynamic analysis, in: 18th Structural Dynamics and Materials Conference, American Institute of Aeronautics and Astronautics, 1977.
[2] R.R. Craig Jr., Coupling of Substructures for Dynamic Analyses - an Overview. 41st Structures, Structural Dynamics, and Materials Conference and Exhibit, American Institute of Aeronautics and Astronautics, 2000.
[3] D. Krattiger, L. Wu, M. Zacharczuk, M. Buck, R.J. Kuether, M.S. Allen, et al., Interface reduction for Hurty/Craig-Bampton substructured models: review and improvements, Mech. Syst. Signal Process. 114 (2019) 579–603.
[4] D. de Klerk, D.J. Rixen, S.N. Voormeeren, General framework for dynamic substructuring: history, review and classification of techniques, AIAA J. 46 (2008) 1169–1181.
[5] R.R. Craig Jr., A Review of Time-Domain and Frequency-Domain Component Mode Synthesis Method, 1985.
[6] R.R. Craig Jr., C.-J. Chang, Substructure Coupling for Dynamic Analysis and Testing, National Aeronautics and Space Administration, 1977.
[7] W. Hurty, Dynamic analysis of structural systems using component modes, AIAA J. 3 (1965) 678–685.
[8] W. Hurty, A Criterion for Selecting Realistic Natural Modes of a Structure, 1967.
[9] R.J. Guyan, Reduction of stiffness and mass matrices, AIAA J. 3 (1965) 380, 380.
[10] R.R. Craig Jr, M. Bampton, C. C, Coupling of substructures for dynamic analyses, AIAA J. 6 (1968) 1313–1319.
[11] M.P. Castanier, Y.-C. Tan, C. Pierre, Characteristic constraint modes for component mode synthesis, AIAA J. 39 (2001) 1182–1187.
[12] R.R. Craig Jr., A.L. Hale, Block-Krylov component synthesis method for structural model reduction, J. Guid. Control Dynam. 11 (1988) 562–570.
[13] R.L. Goldman, Vibration analysis by dynamic partitioning, AIAA J. 7 (1969) 1152–1154.
[14] J. Herrmann, M. Maess, L. Gaul, Substructuring including interface reduction for the efficient vibro-acoustic simulation of fluid-filled piping systems, Mech. Syst. Signal Process. 24 (2010) 153–163.
[15] R.M. Hintz, Analytical methods in component modal synthesis, AIAA J. 13 (1975) 1007–1016.
[16] R.H. MacNeal, A hybrid method of component mode synthesis, Comput. Struct. 1 (1971) 581–601.
[17] D.J. Rixen, A dual Craig–Bampton method for dynamic substructuring, J. Comput. Appl. Math. 168 (2004) 383–391.

[18] S. Rubin, Improved component-mode representation for structural dynamic analysis, AIAA J. 13 (1975) 995–1006.
[19] W.-H. Shyu, Z.-D. Ma, G.M. Hulbert, A new component mode synthesis method: quasi-static mode compensation, Finite Elem. Anal. Des. 24 (1997) 271–281.
[20] D.M. Tran, Component mode synthesis methods using interface modes. Application to structures with cyclic symmetry, Comput. Struct. 79 (2001) 209–222.
[21] L. Wu, P. Tiso, F. van Keulen, Interface reduction with multilevel craig–bampton substructuring for component mode synthesis, AIAA J. 56 (2018) 2030–2044.
[22] J.-G. Kim, P.-S. Lee, An enhanced Craig-Bampton method, Int. J. Numer. Methods Eng. 103 (2015) 79–93.
[23] S.M. Kim, J.-G. Kim, S.-W. Chae, K.C. Park, Evaluating mode selection methods for component mode synthesis, AIAA J. 54 (2016) 2852–2863.
[24] S.M. Kim, J.-G. Kim, K.C. Park, S.-W. Chae, A component mode selection method based on a consistent perturbation expansion of interface displacement, Comput. Methods Appl. Mech. Eng. 330 (2018) 578–597.
[25] J. Gu, Z.-D. Ma, G.M. Hulbert, A new load-dependent Ritz vector method for structural dynamics analyses: quasi-static Ritz vectors, Finite Elem. Anal. Des. 36 (2000) 261–278.
[26] P. Léger, E.L. Wilson, R.W. Clough, The Use of Load Dependent Vectors for Dynamic and Earthquake Analyses: Earthquake Engineering Research Center, College of Engineering, University, 1986.
[27] G.H. Yoon, Toward a multifrequency quasi-static Ritz vector method for frequency-dependent acoustic system application, Int. J. Numer. Methods Eng. 89 (2012) 1451–1470.
[28] G.H. Yoon, J.H. Kim, K.O. Jung, J.W. Jung, Transient quasi-static Ritz vector (TQSRV) method by Krylov subspaces and eigenvectors for efficient contact dynamic finite element simulation, Appl. Math. Model. 39 (2015) 2740–2762.
[29] E.L. Wilson, M.-W. Yuan, J.M. Dickens, Dynamic analysis by direct superposition of Ritz vectors, Earthq. Eng. Struct. Dynam. 10 (1982) 813–821.
[30] A.A. Abdallah, A.A. Huckelbridge, Boundary flexibility method of component mode synthesis using static Ritz vectors, Comput. Struct. 35 (1990) 51–61.
[31] W.-H. Shyu, J. Gu, G.M. Hulbert, Z.-D. Ma, On the use of multiple quasi-static mode compensation sets for component mode synthesis of complex structures, Finite Elem. Anal. Des. 35 (2000) 119–140.
[32] H.S. Koh, J.H. Kim, G.H. Yoon, Efficient topology optimization of multicomponent structure using substructuring-based model order reduction method, Comput. Struct. 228 (2020), 106146.
[33] K.-J. Bathe, Finite Element Procedures, Klaus-Jurgen Bathe, 2006.
[34] B. Nour-Omid, R.W. Clough, Short communication block lanczos method for dynamic analysis of structures, Earthq. Eng. Struct. Dynam. 13 (1985) 271–275.